Element-Selective Probing of Ultrafast Ferromagnetic-Antiferromagnetic Order Dynamics in Fe/CoO Bilayers

Chowdhury S. Awsaf,[1] Sangeeta Thakur,[1] Markus Weißenhofer,[1,2] Jendrik Gördes,[1] Marcel Walter,[1] Mohamad-Assaad Mawass,[3,*] Niko Pontius,[3] Christian Schüßler-Langeheine,[3] Peter M. Oppeneer,[2] and Wolfgang Kuch[1,†]

[1]*Institut für Experimentalphysik, Freie Universität Berlin, Arnimallee 14, 14195 Berlin, Germany*
[2]*Department of Physics and Astronomy, Uppsala University, Box 516, 75120 Uppsala, Sweden*
[3]*Helmholtz-Zentrum Berlin für Materialien und Energie, Albert-Einstein-Straße 15, 12489 Berlin, Germany*

(Received 26 August 2024; revised 24 November 2025; accepted 25 February 2026; published 27 March 2026)

The ultrafast magnetization dynamics of an epitaxial Fe/CoO bilayer on Ag(001) is examined in an element-resolved way by resonant soft-x-ray reflectivity. The transient magnetic linear dichroism at the Co L_2 edge and the magnetic circular dichroism at the Fe L_3 edge measured in reflection in a pump–probe experiment with 120 fs temporal resolution show the loss of antiferromagnetic and ferromagnetic order in CoO and Fe, respectively, both within 300 fs after excitation with 60 fs light pulses of 800 and 400 nm wavelengths. A comparison to spin-dynamics simulations using an atomistic spin model shows that direct energy transfer from the laser-excited electrons in Fe to the magnetic moments in CoO provides the dominant demagnetization channel in the case of 800-nm excitation.

DOI: 10.1103/gcwk-tsj5

The discovery of ultrafast magnetization dynamics by Beaurepaire *et al.* [1] in ferromagnetic (FM) Ni has propelled scientists to investigate emergent ultrafast magnetic phenomena and theorize their possible explanations [2–14]. In recent times, antiferromagnetic (AFM) films have shown great promise for potential applications in memory [15–18] and ultrafast spintronic devices [19–22]. Antiparallel sublattice magnetization eliminates the necessity for overall angular momentum dissipation, resulting in faster magnetization dynamics [23,24]. Moreover, AFMs can be used to tune the magnetic properties of adjacent ferromagnetic films in FM/AFM hybrid layers, for example, to approach specific functionalities. In the ultrafast regime, FM/AFM systems are interesting from a fundamental viewpoint with respect to the interplay of the different local and nonlocal mechanisms [25,26] as well as the magnetic coupling at the interface that may govern the ultrafast response of the system [27]. While the static interaction between the FM and AFM layers has been extensively studied in several systems in the past, little is known about the ultrafast dynamic response of FM/AFM layered systems, despite the importance of interface effects [28]. This is mainly due to the zero net magnetic moment of AFMs, which hampers investigations in general, and time-resolved studies in particular, since it excludes commonly used methods detecting the ultrafast temporal evolution of the total magnetic moment. A method that allows for detecting antiferromagnetic spin order in a time-resolved and element-selective way is required.

Magnetic linear dichroism is such a method that can be used to characterize collinear AFM order. Although typically being much smaller than its circular counterpart, it has been used in the visible-light regime to study the temporal evolution of spin order in CuMnAs or CoO films [29,30]. For the investigation of AFM/FM layered systems, however, elemental specificity is mandatory to separate the signals from the two layers, which is not provided by visible light. Elemental specificity, on the other hand, is routinely achieved in the soft-x-ray regime, where one takes advantage of the differences of elemental absorption energies. Time-resolved x-ray-spectroscopic studies on element-specific AFM order so far have utilized femtosecond soft-x-ray resonant diffraction [7,11,23,24]. Thereby, a relatively large unit cell of the AFM order, comparable to the wavelength of the incident x-rays, is required. This does not work for AFM materials with small magnetic unit cells like collinear AFMs, when the size of the magnetic unit cell is smaller than half of the wavelength of the resonant soft x rays, which is in particular the case for many important 3*d* transition-metal systems.

*Present address: Department of Mathematics and Physics, American University of Ras Al Khaimah, Ras Al Khaimah, United Arab Emirates.

†Contact author: kuch@physik.fu-berlin.de

In this Letter, we employ time-resolved x-ray magnetic linear dichroism in resonant soft-x-ray reflectivity (R-XMLD) [31] to observe the ultrafast dynamics of AFM spins in a single-crystalline CoO film in an Fe/CoO bilayer. R-XMLD, in the same way as XMLD in absorption, probes the difference between the dielectric tensor elements parallel and orthogonal to the x-ray polarization induced by the magnetic moments; see Supplemental Material (SM) [32]. This is even in M, to lowest order proportional to M^2. In AFM materials, M refers to the sublattice magnetization.

We detect the element-resolved dynamic response of the AFM CoO layer and juxtapose it with the demagnetization in the adjacent FM Fe layer, obtained from time-resolved x-ray magnetic circular dichroism in reflection (R-XMCD) [61]. By doing so, we address the important questions of how and on which timescales the optical excitation of an FM/AFM bilayer is transferred between the two layers and into the magnetic subsystems. Exciting both layers simultaneously or only one of them by using pump pulses of 800 or 400 nm wavelength, where the corresponding photon energies are below and above the electronic band gap of CoO [30,62], allows for differentiating the role of different transfer paths.

Interestingly, both layers demonstrate an ultrafast reduction of magnetic order with similar time constants of about 200–400 fs at both pump wavelengths. At the 800 nm pump, the excitation in the CoO layer must be entirely transferred from outside the CoO layer, mainly the Fe layer, as the 800 nm pump photon energy of 1.55 eV is smaller than the CoO bandgap, while at the 400 nm pump, a comparison of the demagnetization amplitudes of both layers shows a significant excitation directly in the CoO layer [63]. We compare the experimental results to atomistic spin-dynamics simulations using the stochastic Landau-Lifshitz-Gilbert (LLG) equation and a temperature model for the different layers and identify a direct energy transfer from the electronic system of the Fe layer to the spin system of the CoO layer across the interface as a relevant mechanism governing the ultrafast spin dynamics of the AFM CoO layer.

A film of 9 ($\pm$0.5) atomic monolayers (ML) average thickness of CoO is grown epitaxially on an Ag(001) surface, following the recipe described in Ref. [33], and capped by 9 ($\pm$1) ML Fe (for details of the sample preparation, see SM [32]). A characteristic XMLD spectrum at the Co $L_{2,3}$ edges in absorption below about 290 K upon turning the polarization axis of linearly polarized x rays of normal incidence by 90° [33] shows a collinearity of the CoO antiferromagnetic spin structure in the film plane. The CoO moments are aligned with the Fe magnetization direction along an Fe $\langle 100 \rangle$ easy axis of magnetization due to a strong coupling at the interface [33,64]. The AFM spin axis can thus be turned by 90° in the sample plane by an external magnetic field via the coupling to the Fe magnetization.

The sample is transferred under ultrahigh vacuum conditions to the synchrotron radiation source BESSY II in Berlin. There, the time-resolved measurements are performed in 10^{-8} mbar pressure, at 200 K with a 120 mT applied field parallel to the sample surface for magnetic saturation, at the Femtoslicing Facility. 60 fs p-polarized pulses of either 800 or 400 nm wavelength are used to pump the sample at a repetition rate of 3 kHz, while subsequent probing is achieved with 100 fs polarized x-ray pulses from the femtoslicing mode of the beamline, probing the sample at 6 kHz, to detect both pumped and unpumped reflected signals alternatingly. The latter are used to normalize the pumped signal. Both pump and probe beams are copropagating (1°–2° apart to filter the pump pulse after reflection) onto the sample at grazing incidence with the pump spot size spanning approximately five times the probe spot size (100 μm) to excite the probed area uniformly. For R-XMLD of CoO and R-XMCD of Fe, we opted for 793.3 eV at the Co L_2 edge and 709.8 eV at the Fe L_3 edge while keeping the same 5° incident grazing angle in both cases in order to maintain identical pump conditions. These energies were chosen to achieve the most efficient measurement condition considering acquisition times for the given angle of incidence [32]. Figure 1(a) shows a

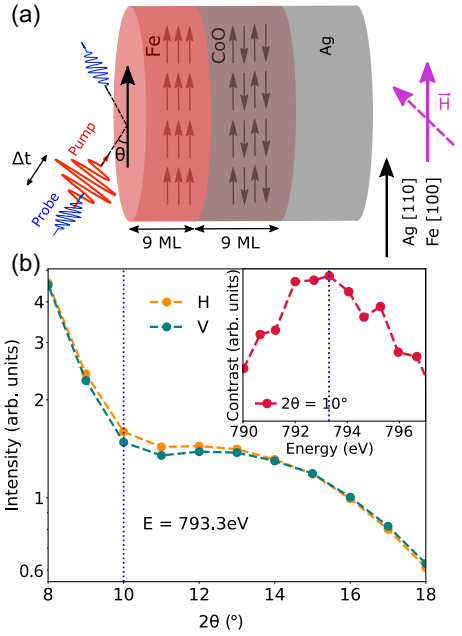

FIG. 1. (a) Sketch of the sample and the experiment. AFM order is probed with linearly s-polarized x-rays tuned to the L_2 resonance of Co, copropagating with a pump pulse, in reflectivity. The magnetic field H is changed by 90° along the sample surface to obtain R-XMLD contrast. (b) Reflected intensity for the parallel and perpendicular directions of the magnetic field as a function of reflection angle at the optimal photon energy for CoO, as established by comparing such scans for different photon energies. The used incidence angle of $\theta = 5°$ is marked by a vertical dashed line. Inset: magnetic contrast as a function of photon energy at the constant angle of $\theta = 5°$. For CoO, the least acquisition time at this angle is attained when the photon energy is 793.3 eV (blue vertical line).

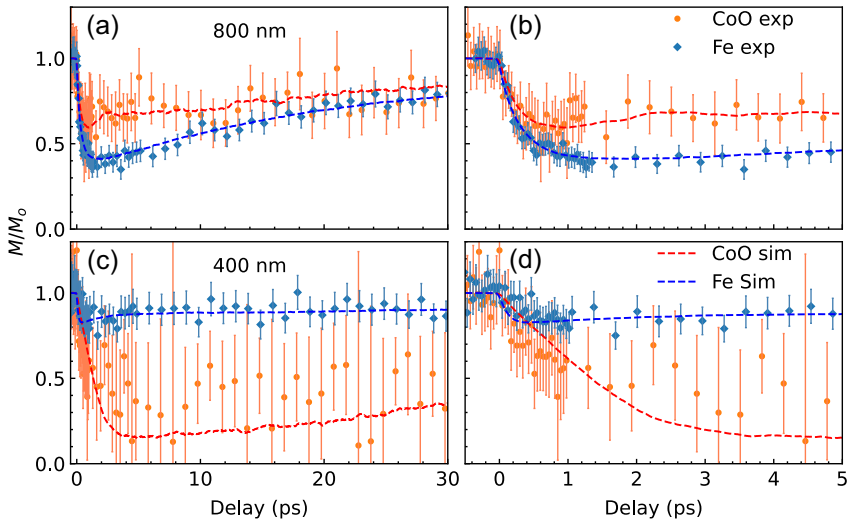

FIG. 2. Magnetization dynamics of CoO and Fe experimentally observed for 800 and 400 nm pump obtained from R-XMLD and R-XMCD measurements as a function of delay time. Both short- and long-range delay-time graphs (right and left panels, respectively) illustrate the different magnetization regimes. The scattered points are the experimental data, and the dashed lines result from a simulation using the atomistic spin model described in the text and schematically depicted in Fig. 3.

sketch of the sample and the experimental configuration, and Fig. 1(b) shows the static magnetic signal at the Co L_2 edge. The x-ray beam was maintained at linear s polarization for the R-XMLD experiment, while the magnetic field was altered by means of the superconducting vector magnet of the beamline in steps of 90° in the sample plane in order to change the magnetic axis of CoO between parallel and perpendicular to the x-ray polarization via the magnetization of the Fe layer. In this way, no structural linear dichroism contributes to the difference signal. For the R-XMCD measurement of Fe, the incident x rays were circularly polarized and the magnetic field direction was reversed by 180° between parallel and antiparallel to the x-ray helicity vector. Effects related to an optically induced transient repopulation of electronic states could in principle also modulate the difference signals at very short time scales well before electron thermalization (≤ 100 fs) [65,66]. As we do not see any signs of sizeable additional contributions to the difference signals on these time scales and the transient changes in the absolute reflectivity are much smaller than in the difference [32], we conclude that the reflectivity changes are predominantly due to R-XMLD and R-XMCD, respectively.

Although the resulting R-XMLD difference amounts to only about 5% of the averaged reflectivity and the sliced synchrotron-radiation probe exhibits about eight orders of magnitude reduced intensity compared to static experiments, it is possible to measure the time evolution of the magnetic signals from Fe and CoO layers at 200 K when pumped at 800 and 400 nm wavelengths with 10 mJ/cm^2 nominal incident fluence (maximum fluence in the laser spot at the surface of the sample). Figure 2 shows the extracted CoO sublattice magnetization and Fe magnetization as a function of delay time after the pump, where in the case of CoO a proportionality of the R-XMLD signal to the square of the sublattice magnetization has been taken into account. Both Fe and CoO exhibit a similarly fast initial drop, which is larger in Fe than in CoO at 800 nm excitation, while at 400 nm Fe demagnetizes less. For a quantitative evaluation, the magnetization dynamics were fitted with a double exponential function convoluted with a 120 fs Gaussian response function in order to describe the fast demagnetization and slower remagnetization of the experimental data within the measured time window [32]. The resulting parameters are summarized in Table I. The extracted demagnetization times are somewhat shorter at 800 nm pump with 200–300 fs compared to 400 nm pump, where 300–450 fs are measured. However, for Fe the experimental uncertainty of the measurement at 400 nm pump is larger than the difference in demagnetization times, while for CoO, it is just at the edge of being significant. The reason for the somewhat different CoO sublattice demagnetization times could be the different mechanisms of excitation of the CoO layer at 800 and 400 nm pump, as will be discussed below.

800 nm photons are below the bandgap of CoO. In a standalone CoO layer, Zheng *et al.* did not observe any response in the time-resolved Voigt-effect signal after 800 nm excitation [30] due to CoO's transparency at this wavelength. Our experimental results for 800 nm excitation, therefore, suggest significant energy transfer to the CoO layer from the other layers, specifically from the Fe layer. This is consistent with previous reports from FM/AFM layered systems. In a work by Ma *et al.*, a CoO/Fe bilayer showed an enhanced precession of the magnetization upon 800 nm excitation compared to a single Fe layer, as detected by time-resolved magneto-optical Kerr effect, which was interpreted as a modulation of the exchange

TABLE I. Demagnetization and remagnetization times (τ_{de} and τ_{re}) and amplitudes (A_{de} and A_{re}) extracted from the experimental data by exponential fits for the CoO sublattice and the Fe transient magnetization at 800 and 400 nm pump wavelengths.

Wavelength/nm	Layer	τ_{de}/fs	A_{de}	τ_{re}/ps	A_{re}
800	CoO	276 ± 47	0.485 ± 0.047	3.7 ± 1.6	0.197 ± 0.043
800	Fe	213 ± 16	0.623 ± 0.007	>20	0.51 ± 0.03
400	CoO	450 ± 130	0.54 ± 0.02	not applicable	0
400	Fe	302 ± 135	0.18 ± 0.02	5.3 ± 3.9	0.08 ± 0.02

anisotropy between Fe and CoO induced by the pump-generated hot electrons in Fe [62]. Wust *et al.* have previously reported comparable findings for a below-bandgap excitation of Pt/NiO bilayers [34]. According to their findings, NiO can effectively demagnetize by an 800 nm laser pump when coated with a Pt layer.

To describe the demagnetization of the Fe/CoO bilayer and the flow of energy between the layers, we model the magnetization dynamics using an atomistic spin model based on stochastic Landau-Lifshitz-Gilbert equations for the spin degrees of freedom coupled to the respective electron and phonon temperatures via Gilbert damping parameters in both layers [35,67]. The Heisenberg Hamiltonian for the spin degrees of freedom is

$$\mathcal{H} = -\sum_{ij} J_{ij} \boldsymbol{S_i} \cdot \boldsymbol{S_j}, \tag{1}$$

where J_{ij} are the coupling constants and $\boldsymbol{S}_i$ are unit vectors along the direction of the magnetic moments of Fe or Co atoms at lattice site i. For simplicity, we treat the system as simple cubic, assume perfect stacking at the interface and restrict the coupling to nearest neighbors, with the coupling constants for CoO and Fe expressed as $J_{ij} = \pm(k_B T_N/1.44)$ and $J_{ij} = (k_B T_c/1.44)$ [36], respectively, with $T_N = 293$ K and $T_c = 1043$ K as the Néel and Curie temperatures for CoO and Fe, respectively. The interfacial coupling J^{if} is taken as a free parameter. The dynamics of the magnetic moments are described using the stochastic LLG equation [37–39],

$$\dot{\boldsymbol{S}}_i = -\frac{\gamma_i}{\mu_i} \boldsymbol{S}_i \times (\boldsymbol{H}_i + \boldsymbol{\zeta}_i) + (\alpha_i^e + \alpha_i^{ph}) \boldsymbol{S}_i \times \dot{\boldsymbol{S}}_i, \tag{2}$$

$$\langle \boldsymbol{\zeta}_i(t) \boldsymbol{\zeta}_i^T(t') \rangle = 2 \frac{\mu_i}{\gamma_i} k_B (\alpha_i^e T_i^e + \alpha_i^{ph} T_i^{ph}) \mathbb{1} \delta_{ij} \delta(t - t'). \tag{3}$$

The first right-hand term in Eq. (2) is the precession torque with gyromagnetic ratio γ_i, spin magnetic moment μ_i, and $\boldsymbol{\zeta}_i(t)$ representing thermal fluctuations to the effective field $\boldsymbol{H}_i = -\partial \mathcal{H}/\partial \boldsymbol{S}_i$ [38]. The second term is the damping torque, where α_i^e and α_i^{ph} are the Gilbert damping constants that couple the respective spin to the electron and phonon subsystems. We assumed a homogeneous distribution of both electron and phonon temperatures in each layer. Furthermore, we took $\alpha_{Fe}^{ph} = 0$, which is reasonable for $3d$ transition metals [40,41].

An energy-conserving temperature model is employed that records the temperature evolution of the electrons (T_e) in Fe and the phonons (T_{ph}) in Fe and CoO; see Fig. 3 and SM [32]. Three energy transfer channels from the Fe to the CoO layer with their respective parameters are considered, as schematically depicted in Fig. 3: the interfacial exchange interaction J^{if} between Fe and CoO spins and the interfacial heat transfer coefficient that couples phonons between Fe and CoO, G_{if}^{ph-ph}; in addition, we introduce a third energy transfer channel by assuming that at the interface, the CoO spins interact with the Fe electron subsystem, similar to Ref. [34]. Within our simulations, this energy transfer, which could stem, e.g., from s–d coupling at the interface [68], was modeled as incoherent by using the temperature of the Fe electrons in the evaluation of the thermal fluctuations for the Co magnetic moments via Eq. (3), with an associated damping coefficient $\alpha_{Fe\to CoO}^{e} = \xi T_{Fe}^{e}$ (see SM [32] for details). In doing so, the linear scaling of $\alpha_{Fe\to CoO}^{e}$ with temperature means that the coupling peaks strongly during the laser pulse (when the electronic temperature reaches thousands of Kelvin). In the model, the substrate only acts as a sink for the phononic energy transport via the coupling constant G_{sink}^{ph-ph} [32]. Induced ferromagnetic Co moments at the Fe/CoO interface [33] act together with the FM Fe layer. Any possible contribution of these to the interface coupling is included in the phenomenological coupling parameters.

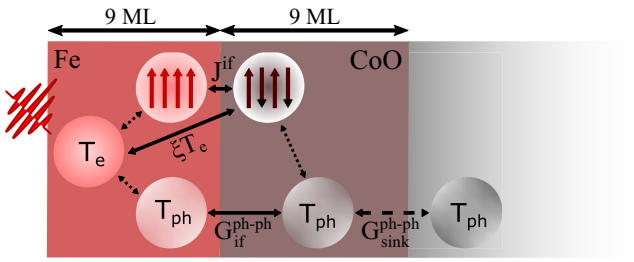

FIG. 3. Representation of different subsystems of the Fe/CoO bilayer on the Ag substrate (see text). The double-headed arrows symbolize the interactions between the different subsystems considered in the model with the solid ones describing the three energy transfer channels from Fe to CoO.

The simulations reveal that phononic and magnonic contributions result only in relatively slow demagnetization of the CoO sublattice magnetization of several picoseconds, and only the electronic channel leads to demagnetization at a subpicosecond timescale [32]. This shows that direct Fe electron–CoO spin coupling plays the dominant role in quenching the CoO antiferromagnetic order when pumped with 800 nm wavelength. By tuning the free parameters α^{e}_{Fe}, J^{if}, α^{ph}_{CoO}, ξ, G^{ph-ph}_{if}, and G^{ph-ph}_{sink}, the model can reproduce both the R-XMLD and R-XMCD data simultaneously as depicted in Figs. 2(a) and 2(b) by dashed lines. Tables SII and SIII of SM [32] present the parameters used to create the lines in Fig. 2. From our model, we speculate that such an ultrashort transfer of excitation could also work between CoO and a nonmagnetic metallic layer. A transfer of excitation from the Ag substrate to the CoO layer, however, would be much less compared to the one from the Fe layer, considering the absorption of the pump pulse in the sample [32].

Implementing the same model, in which the CoO layer is exclusively excited via energy transfer from the Fe layer, to the 400 nm pump data resulted in significantly lower demagnetization of CoO than experimentally observed. Because of the relatively small demagnetization amplitude of the Fe layer at 400 nm, see Fig. 2, the Co R-XMLD signal would then reduce only by 10%–15% compared to the observed 80% [32]. We therefore have to consider a direct excitation of the CoO layer by 400 nm photons, corresponding to 3.1 eV photon energy, which is responsible for the major part of the quench of AFM order in CoO when pumped at 400 nm. At that wavelength, photons can excite electrons from O $2p$ to Co $3d$ states, and spin transfer can occur between adjacent Co sites due to the AFM alignment [30,62].

It is *a priori* not clear how to include such a direct excitation of CoO into our model. One possibility, which we implement here to demonstrate that the experimental data is consistent with the excitation of the CoO layer, is to include an electron temperature of CoO and a finite coupling of CoO spins to CoO electrons, α^{e}_{CoO}, into the model described above (see SM [32]). We use linearized electron heat capacities $C^{e}_{CoO} = \gamma^{e}_{CoO} T^{e}_{CoO}$, although the Sommerfeld model of linear electron heat capacity for metals may be an overestimation for CoO, and a constant (temperature-independent) damping parameter α^{e}_{CoO}. By tuning the relevant parameters, we can replicate the experimental results, as demonstrated in Figs. 2(c) and 2(d). The parameters are presented in Tables SII–SIV in SM [32]. We emphasize that this is only one out of several possible scenarios to model the photoexcitation of CoO, but it shows that such a direct excitation of CoO by the laser pulse explains the experimental result, in particular the larger demagnetization amplitude of CoO compared to that of Fe.

In principle spin transport between the layers could also be discussed as a possibility to explain the different demagnetization amplitudes of CoO and Fe at 400 nm pump. Kumberg *et al.* [25] suggest that magnetic FM/AFM stacks with collinear spin axes can facilitate the entry of minority spin currents into the FM and the transfer of majority spins into the AFM layer, leading to its faster demagnetization of the FM layer. However, this is in contrast to the observed smaller Fe demagnetization (Fig. 2) at 3.1 eV pump. For this, one would need to assume a spin current with a preference for transferring minority electrons from Fe into the CoO or spin-polarized electrons from CoO to Fe with Fe majority spin. We thus expect that spin transport between the layers does not play a major role here.

The different demagnetization amplitudes of Fe at the two different pump wavelengths could be due to a systematic deviation of the pump intensity within the probe spot in the two optical setups used for pumping from the nominally identical fluences [32]. This would be in line with the simulations, where we need to assume a three times lower absorption per atom in the Fe layer in the case of 400-nm excitation compared to 800-nm excitation to match the experimental data [32]. We can also not fully exclude the possibility that there is some other backaction of the CoO layer on the Fe layer besides the AFM–FM exchange coupling at the interface already included in our simulations which reduces the Fe demagnetization amplitude.

Despite the absence of any need to dissipate angular momentum, even at direct excitation of the CoO layer at 400 nm pump the CoO sublattice magnetization does not demagnetize faster than the one of Fe and takes even slightly longer than for CoO at 800 nm pump. The possibly longer time constant of the CoO sublattice demagnetization at 400 nm pump compared to 800 nm pump could be related to the different excitation mechanisms. The observed ultrafast transfer channel from Fe electrons to CoO spins at 800 nm pump obviously works on a time constant not significantly longer than the one of the Fe demagnetization. We speculate that, after direct electronic above-bandgap excitation of the CoO layer at 400 nm pump, transfer to and thermalization with the CoO spin system takes slightly longer, with one reason being the presence of the band gap.

To conclude, using time-resolved XMLD in soft-x-ray reflectivity with 120 fs temporal resolution, we observed the ultrafast spin dynamics in CoO after excitation of an Fe/CoO bilayer by 60 fs pulses of 800 and 400 nm wavelengths on an element-resolved basis. This allows for comparing it with the corresponding element- and time-resolved R-XMCD of the Fe layer to investigate the ultrafast AFM and FM demagnetizations and the interfacial transfer of excitation between the AFM CoO and the FM Fe layer. We find that CoO AFM and Fe FM orders demagnetize similarly fast. Our atomistic spin-dynamics model with stochastic LLG shows that energy transfer via the coupling of hot Fe electrons to CoO spins is the primary mechanism for the rapid quenching of CoO magnetic moments on the order of 300 fs for excitation below the band gap of CoO. The loss of AFM order in the CoO layer is thus entirely due to energy transfer from the interface,

which spreads with the time constant of 276 fs through the entire 9-ML film of CoO. In the case of above-bandgap excitation at 400 nm pump, the magnetic order in CoO reduces much more than the one in Fe, which can only be explained by considering the direct excitation of CoO electrons at that wavelength. Including this in the atomistic simulations describes the experimental observation at 400 nm pump. Our Letter further advocates that the elemental resolution of R-XMLD makes it a promising option for time-resolved magnetization research of AFMs and AFM heterostructures and we expect that it will open a new pathway for studying the ultrafast magnetization dynamics in AFMs in the near future.

Acknowledgments—This work was supported by the Deutsche Forschungsgemeinschaft via the CRC/TRR 227 "Ultrafast Spin Dynamics," Project-ID No. 328545488, Projects A03, A07, and Z. We further acknowledge support from the K. and A. Wallenberg Foundation (Grants No. 2022.0079 and No. 2023.0336). We thank Helmholtz-Zentrum Berlin for the allocation of synchrotron radiation beam time and I. Gelen for help with the sample preparation chamber. Computational resources were provided by the National Academic Infrastructure for Supercomputing in Sweden (NAISS) at NSC Linköping partially funded by the Swedish Research Council through Grant Agreement No. 2022-06725.

Data availability—The data that support the findings of this article are openly available [69].

[1] E. Beaurepaire, J.-C. Merle, A. Daunois, and J.-Y. Bigot, Ultrafast spin dynamics in ferromagnetic nickel, Phys. Rev. Lett. **76**, 4250 (1996).
[2] B. Koopmans, G. Malinowski, F. Dalla Longa, D. Steiauf, M. Fähnle, T. Roth, M. Cinchetti, and M. Aeschlimann, Explaining the paradoxical diversity of ultrafast laser-induced demagnetization, Nat. Mater. **9**, 259 (2010).
[3] M. Battiato, K. Carva, and P. M. Oppeneer, Superdiffusive spin transport as a mechanism of ultrafast demagnetization, Phys. Rev. Lett. **105**, 027203 (2010).
[4] E. Carpene, E. Mancini, C. Dallera, M. Brenna, E. Puppin, and S. De Silvestri, Dynamics of electron-magnon interaction and ultrafast demagnetization in thin iron films, Phys. Rev. B **78**, 174422 (2008).
[5] M. Krauß, T. Roth, S. Alebrand, D. Steil, M. Cinchetti, M. Aeschlimann, and H. C. Schneider, Ultrafast demagnetization of ferromagnetic transition metals: The role of the Coulomb interaction, Phys. Rev. B **80**, 180407(R) (2009).
[6] J. K. Dewhurst, P. Elliott, S. Shallcross, E. K. U. Gross, and S. Sharma, Laser-induced intersite spin transfer, Nano Lett. **18**, 1842 (2018).
[7] K. Holldack, N. Pontius, E. Schierle, T. Kachel, V. Soltwisch, R. Mitzner, T. Quast, G. Springholz, and E. Weschke, Ultrafast dynamics of antiferromagnetic order studied by femtosecond resonant soft x-ray diffraction, Appl. Phys. Lett. **97**, 062502 (2010).
[8] A. Kirilyuk, A. V. Kimel, and T. Rasing, Ultrafast optical manipulation of magnetic order, Rev. Mod. Phys. **82**, 2731 (2010).
[9] A. Kirilyuk, A. V. Kimel, and T. Rasing, Laser-induced magnetization dynamics and reversal in ferrimagnetic alloys, Rep. Prog. Phys. **76**, 026501 (2013).
[10] J. Walowski and M. Münzenberg, Perspective: Ultrafast magnetism and THz spintronics, J. Appl. Phys. **120**, 140901 (2016).
[11] M. Buzzi, M. Först, R. Mankowsky, and A. Cavalleri, Probing dynamics in quantum materials with femtosecond x-rays, Nat. Rev. Mater. **3**, 299 (2018).
[12] K. Carva, P. Baláž, and I. Radu, *Laser-Induced Ultrafast Magnetic Phenomena*, in Handbook of Magnetic Materials (Elsevier, New York, 2017), Vol. 26, pp. 291–463.
[13] C. Wang and Y. Liu, Ultrafast optical manipulation of magnetic order in ferromagnetic materials, Nano Converg. **7**, 1 (2020).
[14] P. Scheid, Q. Remy, S. Lebègue, G. Malinowski, and S. Mangin, Light induced ultrafast magnetization dynamics in metallic compounds, J. Magn. Magn. Mater. **560**, 169596 (2022).
[15] X. Marti *et al.*, Room-temperature antiferromagnetic memory resistor, Nat. Mater. **13**, 367 (2014).
[16] P. Wadley *et al.*, Electrical switching of an antiferromagnet, Science **351**, 587 (2016).
[17] D. Kriegner, K. Výborný, K. Olejník, H. Reichlová, V. Novák, X. Marti, J. Gazquez, V. Saidl, P. Němec, V. V. Volobuev, G. Springholz, V. Holý, and T. Jungwirth, Multiple-stable anisotropic magnetoresistance memory in antiferromagnetic MnTe, Nat. Commun. **7**, 11623 (2016).
[18] K. Olejník, V. Schuler, X. Martí, V. Novák, Z. Kašpar, P. Wadley, R. P. Campion, K. W. Edmonds, B. L. Gallagher, J. Garcés, M. Baumgartner, P. Gambardella, and T. Jungwirth, Antiferromagnetic CuMnAs multi-level memory cell with microelectronic compatibility, Nat. Commun. **8**, 15434 (2017).
[19] T. Jungwirth, X. Marti, P. Wadley, and J. Wunderlich, Antiferromagnetic spintronics, Nat. Nanotechnol. **11**, 231 (2016).
[20] V. Baltz, A. Manchon, M. Tsoi, T. Moriyama, T. Ono, and Y. Tserkovnyak, Antiferromagnetic spintronics, Rev. Mod. Phys. **90**, 015005 (2018).
[21] P. Němec, M. Fiebig, T. Kampfrath, and A. V. Kimel, Antiferromagnetic opto-spintronics, Nat. Phys. **14**, 229 (2018).
[22] D. Xiong, Y. Jiang, K. Shi, A. Du, Y. Yao, Z. Guo, D. Zhu, K. Cao, S. Peng, W. Cai, D. Zhu, and W. Zhao, Antiferromagnetic spintronics: An overview and outlook, Fundam. Res. **2**, 522 (2022).
[23] L. Rettig, C. Dornes, N. Thielemann-Kühn, N. Pontius, H. Zabel, D. L. Schlagel, T. A. Lograsso, M. Chollet, A. Robert, M. Sikorski, S. Song, J. M. Glownia, C. Schüßler-Langeheine, S. L. Johnson, and U. Staub, Itinerant and localized magnetization dynamics in antiferromagnetic Ho, Phys. Rev. Lett. **116**, 257202 (2016).
[24] N. Thielemann-Kühn, D. Schick, N. Pontius, C. Trabant, R. Mitzner, K. Holldack, H. Zabel, A. Föhlisch, and C. Schüßler-Langeheine, Ultrafast and energy-efficient

quenching of spin order: Antiferromagnetism beats ferromagnetism, Phys. Rev. Lett. **119**, 197202 (2017).
[25] I. Kumberg, E. Golias, N. Pontius, R. Hosseinifar, K. Frischmuth, I. Gelen, T. Shinwari, S. Thakur, C. Schüßler-Langeheine, P. M. Oppeneer, and W. Kuch, Accelerating the laser-induced demagnetization of a ferromagnetic film by antiferromagnetic order in an adjacent layer, Phys. Rev. B **102**, 214418 (2020).
[26] E. Golias, I. Kumberg, I. Gelen, S. Thakur, J. Gördes, R. Hosseinifar, Q. Guillet, J. K. Dewhurst, S. Sharma, C. Schüßler-Langeheine, N. Pontius, and W. Kuch, Ultrafast optically induced ferromagnetic state in an elemental antiferromagnet, Phys. Rev. Lett. **126**, 107202 (2021).
[27] A. Eschenlohr, Spin dynamics at interfaces on femtosecond timescales, J. Phys. Condens. Matter **33**, 013001 (2020).
[28] F. Hellman *et al.*, Interface-induced phenomena in magnetism, Rev. Mod. Phys. **89**, 025006 (2017).
[29] V. Saidl *et al.*, Optical determination of the Néel vector in a CuMnAs thin-film antiferromagnet, Nat. Photonics **11**, 91 (2017).
[30] Z. Zheng, J. Y. Shi, Q. Li, T. Gu, H. Xia, L. Q. Shen, F. Jin, H. C. Yuan, Y. Z. Wu, L. Y. Chen, and H. B. Zhao, Magneto-optical probe of ultrafast spin dynamics in antiferromagnetic CoO thin films, Phys. Rev. B **98**, 134409 (2018).
[31] P. M. Oppeneer, H.-C. Mertins, D. Abramsohn, A. Gaupp, W. Gudat, J. Kuneš, and C. M. Schneider, Buried antiferromagnetic films investigated by X-ray magneto-optical reflection spectroscopy, Phys. Rev. B **67**, 052401 (2003).
[32] See Supplemental Material at http://link.aps.org/supplemental/10.1103/gcwk-tsj5 for details of sample preparation, beamline parameters, simulations and the parameters, which includes Refs. [31,33–60].
[33] R. Abrudan, J. Miguel, M. Bernien, C. Tieg, M. Piantek, J. Kirschner, and W. Kuch, Structural and magnetic properties of epitaxial Fe/CoO bilayers on Ag(001), Phys. Rev. B **77**, 014411 (2008).
[34] S. Wust, C. Seibel, H. Meer, P. Herrgen, C. Schmitt, L. Baldrati, R. Ramos, T. Kikkawa, E. Saitoh, O. Gomonay, J. Sinova, Y. Mokrousov, H. C. Schneider, M. Kläui, B. Rethfeld, B. Stadtmüller, and M. Aeschlimann, Indirect optical manipulation of the antiferromagnetic order of insulating NiO by ultrafast interfacial energy transfer, arXiv:2205.02686.
[35] U. Nowak, Classical spin models, in *Handbook of Magnetism and Advanced Magnetic Materials*, edited by H. Kronmüller and S. Parkin (John Wiley & Sons, Ltd, New York, 2007).
[36] D. A. Garanin, Self-consistent Gaussian approximation for classical spin systems: Thermodynamics, Phys. Rev. B **53**, 11593 (1996).
[37] L. D. Landau and E. M. Lifshitz, On the theory of the dispersion of magnetic permeability in ferromagnetic bodies, Phys. Z. Sowjet. **8**, 153 (1935).
[38] W. F. Brown, Thermal fluctuations of a single-domain particle, Phys. Rev. **130**, 1677 (1963).
[39] T. L. Gilbert, A phenomenological theory of damping in ferromagnetic materials, IEEE Trans. Magn. **40**, 3443 (2004).
[40] D. Zahn, F. Jakobs, Y. W. Windsor, H. Seiler, T. Vasileiadis, T. A. Butcher, Y. Qi, D. Engel, U. Atxitia, J. Vorberger, and R. Ernstorfer, Lattice dynamics and ultrafast energy flow between electrons, spins, and phonons in a 3*d* ferromagnet, Phys. Rev. Res. **3**, 023032 (2021).
[41] D. Zahn, F. Jakobs, H. Seiler, T. A. Butcher, D. Engel, J. Vorberger, U. Atxitia, Y. W. Windsor, and R. Ernstorfer, Intrinsic energy flow in laser-excited 3*d* ferromagnets, Phys. Rev. Res. **4**, 013104 (2022).
[42] H.-C. Mertins, P. M. Oppeneer, J. Kuneš, A. Gaupp, D. Abramsohn, and F. Schäfers, Observation of the X-ray magneto-optical Voigt effect, Phys. Rev. Lett. **87**, 047401 (2001).
[43] S. Macke and E. Goering, Magnetic reflectometry of heterostructures, J. Phys. Condens. Matter **26**, 363201 (2014).
[44] https://www.remagx.org/.
[45] B. Henke, E. Gullikson, and J. Davis, X-ray interactions: Photoabsorption, scattering, transmission, and reflection at E = 50–30000 eV, Z = 1–92, At. Data Nucl. Data Tables **54**, 181 (1993).
[46] S. Brück, Magnetic resonant reflectometry on exchange bias systems, Ph.D. thesis, Universität Stuttgart, 2009, p. 92 ff, 10.18419/opus-6723.
[47] I. Kumberg, E. Golias, S. E. Hadjadj, R. Hosseinifar, S. Thakur, T. Shinwari, I. Gelen, N. Pontius, C. Schüßler-Langeheine, C. von Korff Schmising, S. Sharma, and W. Kuch, Ultrafast laser-induced magneto-optical changes in resonant magnetic x-ray reflectivity, Phys. Rev. B **108**, 054439 (2023).
[48] J. Kuneš and P. M. Oppeneer, Anisotropic x-ray magnetic linear dichroism at the $L_{2,3}$ edges of cubic Fe, Co, and Ni: *Ab initio* calculations and model theory, Phys. Rev. B **67**, 024431 (2003).
[49] K. Ohta and H. Ishida, Matrix formalism for calculation of the light beam intensity in stratified multilayered films, and its use in the analysis of emission spectra, Appl. Opt. **29**, 2466 (1990).
[50] P. B. Johnson and R. W. Christy, Optical constants of transition metals: Ti, V, Cr, Mn, Fe, Co, Ni, and Pd, Phys. Rev. B **9**, 5056 (1974).
[51] P. B. Johnson and R. W. Christy, Optical constants of the noble metals, Phys. Rev. B **6**, 4370 (1972).
[52] R. J. Powell and W. E. Spicer, Optical properties of NiO and CoO, Phys. Rev. B **2**, 2182 (1970).
[53] T. Chirac, J.-Y. Chauleau, P. Thibaudeau, O. Gomonay, and M. Viret, Ultrafast antiferromagnetic switching in NiO induced by spin transfer torques, Phys. Rev. B **102**, 134415 (2020).
[54] U. Ritzmann, P. Baláž, P. Maldonado, K. Carva, and P. M. Oppeneer, High-frequency magnon excitation due to femtosecond spin-transfer torques, Phys. Rev. B **101**, 174427 (2020).
[55] M. Weißenhofer, F. Foggetti, U. Nowak, and P. M. Oppeneer, Néel vector switching and terahertz spin-wave excitation in Mn_2Au due to femtosecond spin-transfer torques, Phys. Rev. B **107**, 174424 (2023).
[56] Y. Tserkovnyak, A. Brataas, and Gerrit E. W. Bauer, Spin pumping and magnetization dynamics in metallic multilayers, Phys. Rev. B **66**, 224403 (2002).

[57] U. Ritzmann, P. M. Oppeneer, and P. Maldonado, Theory of out-of-equilibrium electron and phonon dynamics in metals after femtosecond laser excitation, Phys. Rev. B **102**, 214305 (2020).

[58] NIST Chemistry Webbook, SRD 69, https://webbook.nist.gov/cgi/cbook.cgi?ID=C1307966&Type=JANAFS&-Table=on (2022) [Accessed: November 24, 2023].

[59] J. Kübler, Magnetic moments of ferromagnetic and antiferromagnetic bcc and fcc iron, Phys. Lett. **81A**, 81 (1981).

[60] D. Herrmann-Ronzaud, P. Burlet, and J. Rossat-Mignod, Equivalent type-II magnetic structures: CoO, a collinear antiferromagnet, J. Phys. C **11**, 2123 (1978).

[61] H.-C. Mertins, D. Abramsohn, A. Gaupp, F. Schäfers, W. Gudat, O. Zaharko, H. Grimmer, and P. M. Oppeneer, Resonant magnetic reflection coefficients at the Fe $2p$ edge obtained with linearly and circularly polarized soft x rays, Phys. Rev. B **66**, 184404 (2002).

[62] X. Ma, F. Fang, Q. Li, J. Zhu, Y. Yang, Y. Z. Wu, H. B. Zhao, and G. Lüpke, Ultrafast spin exchange-coupling torque via photo-excited charge-transfer processes, Nat. Commun. **6**, 8800 (2015).

[63] Direct excitation of the CoO layer at 800 nm pump across the band gap by two-photon absorption can be ruled out from the fluence dependence of the CoO sublattice demagnetization; see Ref. [32].

[64] J. Miguel, R. Abrudan, M. Bernien, M. Piantek, C. Tieg, J. Kirschner, and W. Kuch, Magnetic domain coupling study in single-crystalline Fe/CoO bilayers, J. Phys. Condens. Matter **21**, 185004 (2009).

[65] K. Carva, D. Legut, and P. M. Oppeneer, Influence of laser-excited electron distributions on the x-ray magnetic circular dichroism spectra: Implications for femtosecond demagnetization in Ni, Europhys. Lett. **86**, 57002 (2009).

[66] K. Yao, F. Willems, C. von Korff Schmising, I. Radu, C. Strüber, D. Schick, D. Engel, A. Tsukamoto, J. K. Dewhurst, S. Sharma, and S. Eisebitt, Distinct spectral response in M-edge magnetic circular dichroism, Phys. Rev. B **102**, 100405(R) (2020).

[67] N. Kazantseva, U. Nowak, R. W. Chantrell, J. Hohlfeld, and A. Rebei, Slow recovery of the magnetisation after a sub-picosecond heat pulse, Europhys. Lett. **81**, 27004 (2007).

[68] W. Chen, M. Sigrist, J. Sinova, and D. Manske, Minimal model of spin-transfer torque and spin pumping caused by the spin Hall effect, Phys. Rev. Lett. **115**, 217203 (2015).

[69] C. S. Awsaf, S. Thakur, M. Weißenhofer, J. Gördes, M. Walter, M.-A. Mawass, N. Pontius, C. Schüßler-Langeheine, P. M. Oppeneer, and W. Kuch, 10.5281/zenodo.15497443 (2026).